Multi-harmonic Multiple-point Collocation: A Method for Finding Periodic Orbits of Strongly Nonlinear Oscillators

Hamid A. Ardeh
ansariardeh@wisc.edu
Department of Mechanical Engineering, University of Wisconsin-Madison

Matthew S. Allen
Department of Engineering Physics, University of Wisconsin-Madison

An iterative method is proposed for finding periodic orbits of strongly nonlinear oscillators. The method combines the strength of analytical approaches, where the candidate solution is assumed in the form of a Fourier series, and the convenience of numerical methods that can be applied to larger systems with strong nonlinearity. The proposed method does not require integration of the vector field over any period of time and examples presented here illustrate that it is faster than traditional collocation algorithms, has a large radius of convergence and is capable of finding several periodic obits in each solution.

1 Introduction

Nonlinearities are important in many engineering structures. For example, consider the pinned-pinned beam shown in Fig.7. As the response amplitude increases the beam must stretch axially to accommodate the bending deformation and this bending/axial coupling introduces a stiffness nonlinearity that can dramatically change the nature of the response, potentially leading to unexpected resonances or even instability and chaos. The lightweight skin panels on aircraft and many other structures exhibit this type of nonlinearity as the displacement amplitude approaches the shell thickness, sometimes at surprisingly small loads (see, e.g. [1]). One of the first steps toward understanding the response of a structure such as this is often an analysis in which the periodic orbits of the nonlinear system are computed. The periodic solutions of the forced, damped system can be computed and used to predict the bent resonances that are characteristic of the nonlinear frequency response of a nonlinear system, or one may instead compute periodic responses of the undamped nonlinear system or the Nonlinear Normal Modes [17], which form the backbone of the nonlinear frequency response. Periodic orbits are also often sought as a first step in studying bifurcation or chaos in nonlinear systems. This work presents a new algorithm that can be used to compute these periodic responses without having to integrate the equations of motion or requiring symbolic manipulation of the equations of motion.

Algorithms that attempt to find periodic orbits of autonomous differential equations can be divided into two categories. The fist class of algorithms use the fact that all periodic functions have closed form approximations such as a Fourier series expansion. These algorithms attempt to fit one of these approximations to a solution of the system and then extract the set $\{y_0, T\}$ from the approximation form. For example, perturbation theory formulates the solution as a series expansion in small parameters [20], but unfortunately this limits the method to weakly nonlinear systems. Averaging methods, such as Harmonic-Balance, rely on a Fourier series expansion to approximate the periodic orbit of the system by averaging (evaluating an integral of the response or the vector field) it over one period. Variational methods can be used for strongly nonlinear systems, however, like perturbation and averaging methods, they rely on analytic procedures to find periodic orbits and are not readily extendable to large systems [7].

A second class of methods finds a set of an initial conditions and a period, i.e. $\{y_0, T\}$, for which, the solution of the system that is initiated at the initial condition y_0 returns to it after the time T[1]. In this sense, a different class of approaches, generally known as multi-point boundary value methods [23], restates the problem of finding periodic orbits of the system

$$\ddot{x} = f(x), x \in \mathbb{R}^n. \tag{1}$$

as finding a point y_0 for which

[1] In this study, we do not consider cases of homoclinic and heteroclinic orbits.

$$y_0 = y(t_0) = \begin{bmatrix} x \\ \dot{x} \end{bmatrix}_{t=t_0} = \begin{bmatrix} x \\ \dot{x} \end{bmatrix}_{t=t_0+T} = y(t_0+T). \quad (2)$$

Algorithms based on this approach are known as shooting (or multiple shooting in general) algorithms. In the case of multiple shooting, the interval $[t_0, t_0+T]$ is divided into M sub-intervals $[t_p, t_{p+1}]$ and consequently the system (1) and the condition (2) and are

$$\ddot{x}_p = f(x_p),\ p = 1,...,M \quad (3)$$

and

$$\begin{bmatrix} x \\ \dot{x} \end{bmatrix}_{\tau=1}^{(p)} = \begin{bmatrix} x \\ \dot{x} \end{bmatrix}_{\tau=0}^{(p+1)} \text{ and } \begin{bmatrix} x \\ \dot{x} \end{bmatrix}_{\tau=0}^{(1)} = \begin{bmatrix} x \\ \dot{x} \end{bmatrix}_{\tau=1}^{(M+1)}, \quad (4)$$
$$p = 1,...,M,\ p \geq 1$$

where $x_p(\tau) = x(t_{p-1} + (t_p - t_{p-1})\tau)$, $\tau = \frac{t-t_{p-1}}{t_p - t_{p-1}}$. In other words, the two points in Eq. ((2)) are augmented by $(M-2)$ intermediate points to help improve the convergence of the solution of the system to a periodic orbit. It is worth pointing out that, since the boundary points are found by integrating the vector field (always) initiated at $y(t_0)$, these approaches implicitly impose the constraint that all the points in (2) (or (4)) must be on the same solution (see Fig.1). Shooting algorithms are widely used to satisfy the mentioned conditions (2) or (4) by minimizing the shooting function, i.e. $\min_{x,\dot{x}} \left(\sum_1^M \left\| \begin{bmatrix} x \\ \dot{x} \end{bmatrix}_{\tau=1}^{(p)} - \begin{bmatrix} x \\ \dot{x} \end{bmatrix}_{\tau=0}^{(p+1)} \right\| \right)$ or its integral, i.e. $\min_{x,\dot{x}} \left(\sum_1^M \int_{t_p}^{t_{p+1}} \left\| \begin{bmatrix} x \\ \dot{x} \end{bmatrix}_{\tau=1}^{(p)} - \begin{bmatrix} x \\ \dot{x} \end{bmatrix}_{\tau=0}^{(p+1)} \right\| dt \right)$. These algorithms are usually paired with the principle of continuation [2, 18] to find a branch of solutions. For example, Peeters et al. recently presented a shooting/continuation algorithm that has proven effective for solving the class of problems that are of interest in this work [21]. While these methods have proven effective in many scenarios, they are sensitive to the initial guesses for the parameters and require repeatedly integrating the equations of motion to find the time response over one period.

The algorithm presented here is somewhat comparable to approaches, such as that used in the software AUTO [9] and MatCont [10], which rely on orthogonal collocation to solve the boundary value problem.

2 Multi-harmonic Multiple-point Collocation

The proposed Multi-Harmonic Multiple-point Collocation (MMC) algorithm uses an approach that resembles the multiple shooting algorithm, but is in fact fundamentally different. In essence, rather than enforcing the periodicity condition in Eq. (2) or (4), the solution is expressed in the form of a Fourier series so that it is automatically periodic with period T . However, we shall see that in order to acheive certain computational gains in the algorithm, this does not necessarily guarantee that the solution(s) obtained have the same period. Specifically, consider a potential solution, $\bar{x}$, that is represented by a Fourier series as follows.

$$\bar{x}(\phi) = \sum_{k=1}^{N} \left\{ \begin{bmatrix} A_{1k} \\ \vdots \\ A_{nk} \end{bmatrix} \cos(k\phi) + \begin{bmatrix} B_{1k} \\ \vdots \\ B_{nk} \end{bmatrix} \sin(k\phi) \right\} \quad (5)$$

The candidate solution is periodic over a nondimensional time base $0 \leq \phi < 2\pi$, where $\phi = \omega t$, $\omega = \frac{2\pi}{T}$ and $T \in \mathbb{R}^+$is the period of the Fourier series. The overbar also emphasizes the fact that this function will not be guaranteed to satisfy the differential equation at every point on the interval $[0, 2\pi]$, as will be explained subsequently.

The proposed algorithm solves for the coefficients $A_{1k}, ...$ and $B_{1k}, ...$ in the candidate solution above by satisfying the following condition at a set of collocation points $\phi_k \in [0, 2\pi]$.

$$\ddot{\bar{x}}(\phi_k) - f(\bar{x}(\phi_k)) = 0,\ k = 1,...,M \quad (6)$$

The goal is to combine the strength of analytical approaches, by using an analytical candidate solution (host) $\bar{x}$, and the convenience of numerical methods, which can be applied to large systems with strong nonlinearity. The solution host can be differentiated analytically, so the MMC condition can be checked by simply evaluating the forcing function, f, at each point. Hence, the MMC condition is an alternative to the conditions (2) or (4), that avoids having to integrate of the vector field over any period of time. However, because one is not required to integrate form one point in time to another, each of the M pairs of collocation points in the MMC condition may end up coming from a different solution of the system. Hence, the overbar on $\bar{x}$ serves as a reminder that $\bar{x}$ is not a solution $x(t)$ of the system but simply a solution host that defines one point on up to M different solutions to the nonlinear system. These concepts are discussed in detail in the following sections.

In order to more fully understand the difference between multiple shooting and MMC, consider a periodic candidate solution host $\bar{y} = \begin{bmatrix} \bar{x} \\ \dot{\bar{x}} \end{bmatrix}$. The periodicity condition in Eq. ((2)) is automatically satisfied by the solution host on the period T, so it might appear that all that remains is to ensure that the solution host satisfies the differential equation using Eq. (6). However, the collocation points have not been forced to pertain to a single solution $y(t)$, so each of the M pairs of points $\bar{y}(\phi_k)$ could in fact correspond to a different solution

with a different period T_k. This is shown schematically in Fig. 1, and also contrasted with multiple shooting, where the candidate solution is forced to be continuous from one subset to the next.

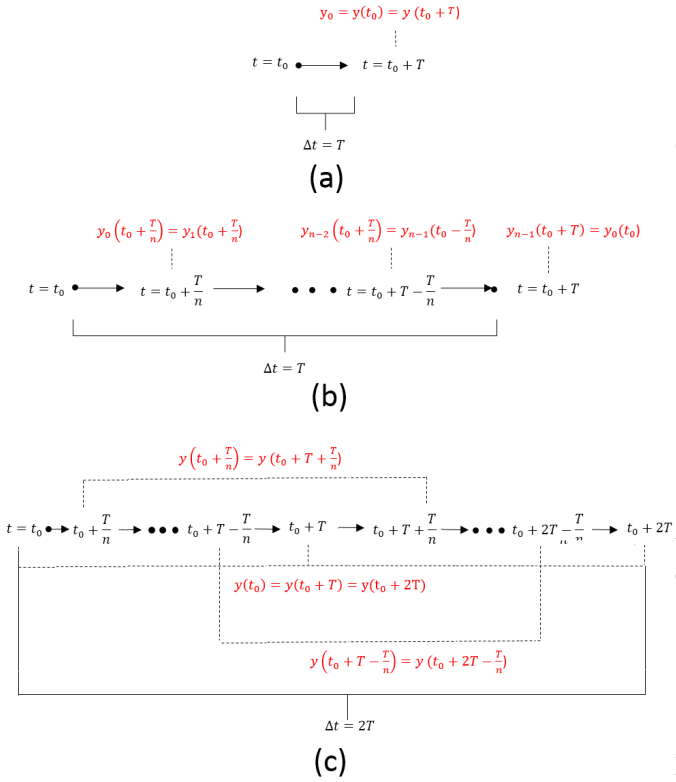

Figure 1. (a) Illustration of two-point collocation condition used in shooting algorithms. (b) Multiple-point collocation condition used in multiple shooting algorithms. (C) Multiple-point collocation condition used in the proposed algorithm. The $2M$ points are used to create M **independent** two-point collocation conditions.

Two iterative algorithms, discussed in Sections 3.1 and 3.2, are presented to adjust the coefficients, $A_{1k}, \ldots$ and $B_{1k}, \ldots$, and the period, T, until the MMC condition is satisfied. The proposed method is exemplified for a simple two dimensional (n=2) and a rather large, ten dimensional (n=10) system in Sections 4 and 5.

2.1 Difference Function

In order to find a solution that satisfies Eq. (6), we define the following difference function, which can be shown to be identical to the periodicity condition in Eq. (2),

$$\delta_k(\bar{x}) = \ddot{\bar{x}}(\phi_k) - f(x(\phi_k)) = 0, k = 1, \ldots, M, \tag{7}$$

where the only difference beteween this and Eq. (6) is that the argument of f is now the true solution to the system. Now, consider the case where $\delta_k \neq 0$. In this regard, suppose that a (yet unknown) solution of the system x and a multi-harmonic candidate solution $\bar{x}$ satisfy Eq. (7) with $x(\frac{\phi_k}{2\pi}T) = \bar{x}(\phi_k)$ but they differ after one period so $x(\frac{2\pi+\phi_k}{2\pi}T) + \delta_k = \bar{x}(\phi_k)$ where $\delta_k \neq 0$ is small. Inserting this into the MMC condition, one can write

$$\ddot{\bar{x}}(\phi_k) - f(\bar{x}(\phi_k) + \delta_k) = 0, \tag{8}$$

or approximately

$$\ddot{\bar{x}}(\phi_k) - f(\bar{x}(\phi_k)) - \mathbb{J}_x^f(\bar{x}(\phi_k))\delta_k \backsimeq 0, \tag{9}$$

and so the difference can be found

$$\delta_k \backsimeq \left[\mathbb{J}_x^f(\bar{x}(\phi_k))\right]^{-1}\left[\ddot{\bar{x}}(\phi_k) - f(\bar{x}(\phi_k))\right] \tag{10}$$

and can finally be expressed in terms of the difference function, $\bar{\delta}_k(\bar{x}) = [\ddot{\bar{x}}(\phi_k) - f(\bar{x}(\phi_k))]$, which depends only on the candidate solution $\bar{x}$.

$$\delta_k = \left[\mathbb{J}_x^f(\bar{x}(\phi_k))\right]^{-1}\bar{\delta}_k(\bar{x}) \tag{11}$$

Hence, as long as $\mathbb{J}_x^f(\bar{x}(\phi_k))$ is not singular at $\bar{x}(\phi_k)$, i.e. f is monotonic[2] at the collocation points $\bar{x}(\phi_k)$, one can conclude that it is possible to reduce $\bar{\delta}_k(\bar{x})$ and as a result when the multi-harmonic multiple-point collocation condition is met at a set of collocation points, i.e.

$$\bar{\delta}_k(\bar{x}) = \ddot{\bar{x}}(\phi_k) - f(\bar{x}(\phi_k)) = 0, k = 1, \ldots, 2M. \tag{12}$$

then each of these points, ϕ_k, on the candidate solution host are also on the solutions of the system that satisfy (7). Equivalently, $\bar{x}(\phi_k)$ collocates with points on a periodic solution of the system, i.e a solution x which satisfies $x(\frac{\phi_k}{2\pi}T) = x(\frac{2\pi+\phi_k}{2\pi}T)$. The condition in Eq. ((12)) then imposes a constraint that plays the same role as integration in multi-point boundary value problem methods by implicitly forcing the candidate solution $\bar{x}$ to collocate with the solution of the system x at finite number of points in the state space. Note that conditions described above are also met if the true solution has a shorter period, for example, $\frac{T}{n}$, where n is an integer. Hence, the solution at each collocation point could also have a different period,T.

[2]The definition of monotonicity used here is derived from Monotone Operator Theory, which is explained in detail in the following references [5, 6, 27]. The general theory can be simplified considerably for the purposes of this work, as outlined in the Appendix.

3 Multi-harmonic Multiple-point Collocation: Numerical Algorithms

In this section we propose two algorithms to modify the candidate host $\bar{x}$ until it satisfies the multi-harmonic multiple-point collocation condition (12).

3.1 Inexact Golden-Section Line Search MMC

Here we propose a steepest descent algorithm augmented by an inexact golden-section line search subroutine. The mentioned inexact line search is performed to find the step-size at each iteration that satisfies Wolfe conditions (to find inexact optimal step-size at each iteration). The immediate and main advantages of using this algorithm is to first to relax the need to calculate the inverse of any slope functions (Jacobian, or Hessian), which is required in Newtonian algorithms, while providing the same level of accuracy in choosing a step-size as is usually associated with Newtonian methods. In this regard we first define a deviation function

$$\begin{aligned} D &= \sum_{i=1}^{2M} \bar{\delta}^T \bar{\delta} \\ &= \sum_{i=1}^{2M} \left[f(\bar{x}(\phi_i)) - \ddot{\bar{x}}(\phi_i) \right]^T \left[f(\bar{x}(\phi_i)) - \ddot{\bar{x}}(\phi_i) \right] \end{aligned} \tag{13}$$

Next, starting from an initial guess $\bar{x}^{(0)}$ determined by $\{C^{(0)}, \omega^{(0)}\}$ where

$$\begin{aligned} C^{(0)} = [A_{11} \cdots A_{1N} | B_{11} \cdots B_{1N} | \\ \cdots | A_{n1} \cdots A_{nN} | | B_{n1} \cdots B_{nN}]_0^T \end{aligned} \tag{14}$$

and $\omega^{(0)}$ is initial guess for the frequency of the multi-harmonic candidate host. We then find the next approximation by navigating the candidate solution $\bar{x}$ in the directions which are functions of the gradient of D with respect to the coefficient vector C, and the frequency ω denoted by g_C^D and g_ω^D respectively. Specifically,

$$\begin{aligned} C^{q+1} &= C^q - r_c v_{C^q}^q \\ \omega^{q+1} &= \omega^q - r_\omega v_{\omega^q}^q. \end{aligned} \tag{15}$$

where $v_{C^k}^k$ and $v_{\omega^k}^k$ are search directions (defined below) and r_c and $r_w = \alpha r_c$, $\alpha \in \mathbb{R}^+$ are the step size control parameters, which are determined using an inexact Golden-Section line search method. The search directions, for both coefficient vector and frequency, are the steepest descent directions at the first step. Subsequent steps, however, are defined recursively by

$$\begin{aligned} v_{C^{k+1}}^{k+1} &= g_{C^{k+1}}^D + diag(\gamma_i^k) v_{C^k}^k, \; v_{C^0}^0 = g_{C^0}^D \\ v_{\omega^{k+1}}^{k+1} &= g_{\omega^{k+1}}^D + \gamma^k v_{\omega^k}^k, \; v_{\omega^0}^0 = g_{\omega^0}^D, \end{aligned} \tag{16}$$

where $\gamma^k \in \mathbb{R}$ is chosen as

$$\begin{aligned} \gamma_{C_i^k}^k &= \frac{\left\| g_{C_i^{k+1}}^D \right\|^2}{(v_{C^k}^k)^T (g_{C_i^{k+1}}^D - g_{C_i^k}^D)} \\ \gamma_{\omega^k}^k &= \frac{(g_{\omega^{k+1}}^D)^2}{(v_{\omega^k}^k)(g_{\omega^{k+1}}^D - g_{\omega^k}^D)}, \end{aligned} \tag{17}$$

This reduces minimization of (13) to a conjugate gradient method minimization problem[14, 12, 13]. Specifically, at each iteration, a minimization problem defined by

$$\min_{r_c^k} D(C^{q+1}, \omega^{q+1}) \tag{18}$$

must be solved to find an optimal step-size r_c^k . However, while an exact solution to Eq. (18) is not available, an inexact solution can be found by finding a step-size r_c^k using a Golden-section line search described by

$$r_c^{k+1} = r_c^k / \alpha_{GS}, \; r_c^0 = r_c^{max} \in \mathbb{R}^+, \tag{19}$$

where $\alpha_{GS} = \frac{1+\sqrt{5}}{2}$ is the golden section ratio, that satisfies the (strong) Wolfe conditions

1. $D(C^{q+1}, \omega^{q+1}) - D(C^q, \omega^q) \leq \delta \left[r_c^k C^{q^T} g_{C^q}^D + \alpha r_c^k \omega^q g_{\omega^q}^D \right]$,
2. $C^q g_{C^{q+1}}^D + \omega^q g_{\omega^{q+1}}^D \geq \sigma \left[C^{q^T} g_{C^q}^D + \omega^q g_{\omega^q}^D \right]$.

in which $0 < \delta < \sigma < 1$. Applying the Wolfe conditions and setting parameters δ and σ ensures that the the deviation function D and its gradients g_C^D and g_ω^D decrease sufficiently at each step. Usually δ is chosen to be very small and σ to be very close to 1. Throughout this study theses parameters are kept constant $\delta = 0.01$, $\sigma = 0.9$ using the suggestions in [14, 12, 22].

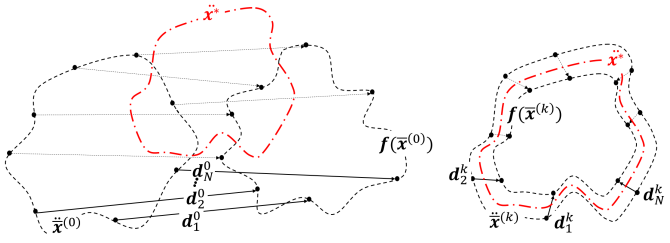

Figure 2. Schematic representation of a case of homogenous convergence. Left: The candidate periodic solution $\bar{x}$ changes its shape in a manner that reduces the sum of the norms of the distance vectors d_i, i.e. the deviation function D. Right: As the deviation function D tends to zero, the candidate solution $\bar{x}$ converges to periodic orbits of the system.

In this regard, defining

$$\Gamma(v^T) = \begin{bmatrix} v^T & 0_{1\times 2N} & \vdots & 0_{1\times 2N} \\ 0_{1\times 2N} & v^T & \ddots & \vdots \\ \vdots & \ddots & \ddots & 0_{1\times 2N} \\ 0_{1\times 2N} & \cdots & 0_{1\times 2N} & v^T \end{bmatrix}, \tag{20}$$

and

$$\begin{aligned} \alpha_m^T &= \big[\cos\phi_m \; 2^2\cos(2\phi_m) \; \cdots \; (N)^2\cos(N\phi_m) \\ &\quad \sin\phi_m \; 2^2\sin(2\phi_m) \; \cdots \; (N)^2\sin(N\phi_m)\big] \\ \beta_m^T &= \big[\cos\phi_m \; \cdots \; \cos(N\phi_m) \\ &\quad \sin\phi_m \; \cdots \; \sin(N\phi_m)\big] \\ \phi_m &= \frac{m}{M}(2\pi) \in [0, 2\pi), \; m = 1, ..., M. \\ \phi_{m+M} &= 2\pi + \phi_m \end{aligned} \tag{21}$$

one can readily show that

$$\begin{aligned} \bar{x}_m^{(k)} &= \Gamma(\beta_m^T)\bar{C}^{(k)} \\ \bar{\delta}_m^{(k)} &= \omega^2\Gamma(\alpha_m^T)\bar{C}^{(k)} + f(\bar{x}_m^{(k)}) \\ \mathbb{J}_C^{\bar{\delta}_m^{(k)}} &= \omega^2\Gamma(\alpha_m^T) + \mathbb{J}_x^f(\bar{x}_m^{(k)})\Gamma(\beta_m^T) \\ \mathbb{J}_\omega^{\bar{\delta}_m^{(k)}} &= 2\omega\Gamma(\alpha_m^T)\bar{C}^{(k)} \end{aligned} \tag{22}$$

where $\mathbb{J}_v^u$ defines the Jacobian of the vector u with respect to the vector v.
Therefore, the gradient vectors can be found as

$$\begin{aligned} g_C &= \nabla_C D = \nabla_C \sum_{i=1}^{2M} (\bar{\delta}_i^T \bar{\delta}_i) = 2\sum_{i=1}^{2M} \left(\mathbb{J}_C^{\bar{\delta}_i}\right)^T \bar{\delta}_i \\ g_\omega &:= \nabla_\omega D = \nabla_\omega \sum_{i=1}^{2M} (\bar{\delta}_i^T \bar{\delta}_i) = 2\sum_{i=1}^{2M} \left(\mathbb{J}_\omega^{\bar{\delta}_i}\right)^T \bar{\delta}_i. \end{aligned} \tag{23}$$

3.2 Newtonian MMC

One can also use a Newtonian algorithm to minimize the vector δ by modifying the candidate solution as

$$\begin{aligned} C^{q+1} &= C^q + \Delta C^q \\ \omega^{q+1} &= \omega^q + \Delta\omega^q. \end{aligned} \tag{24}$$

where ΔC^q and $\Delta\omega^q$ are computed by solving a set of overdetermined linear equations defined by

$$\begin{aligned} [\mathbb{J}_{C^q}^{\bar{\delta}_i^q} \mathbb{J}_{\omega^q}^{\bar{\delta}_i^q}] \begin{bmatrix} \Delta C_i^q \\ \Delta\omega_i^q \end{bmatrix} &= \bar{\delta}_i^q, \; i = 1, ..., 2M \\ \begin{bmatrix} \Delta C_i^q \\ \Delta\omega_i^q \end{bmatrix} = \begin{bmatrix} \Delta C_j^q \\ \Delta\omega_j^q \end{bmatrix} &= \begin{bmatrix} \Delta C^q \\ \Delta\omega^q \end{bmatrix}, \; i, j = 1, ..., 2M \end{aligned} \tag{25}$$

Note that the constraint condition is enforced to guarantee uniqueness of the solution host (defined by C^q and ω^q) in each iteration. The system in (25) can be further simplified by averaging to obtain

$$[\sum_{i=1}^{2M} \mathbb{J}_{C^q}^{\bar{\delta}_i^q} \sum_{i=1}^{2M} \mathbb{J}_{\omega^q}^{\bar{\delta}_i^q}] \begin{bmatrix} \Delta C^q \\ \Delta\omega^q \end{bmatrix} = \sum_{i=1}^{2M} \bar{\delta}_i^q \tag{26}$$

which can be solved for ΔC^q and $\Delta\omega^q$ using the Moore-Penrose inverse. In another (more traditional) approach one can enforce uniqueness of the solution host by recasting the system in (25) as

$$\begin{bmatrix} \mathbb{J}_{C^q}^{\bar{\delta}_1^q} & \mathbb{J}_{\omega^q}^{\bar{\delta}_1^q} \\ \vdots & \vdots \\ \mathbb{J}_{C^q}^{\bar{\delta}_{2M}^q} & \mathbb{J}_{\omega^q}^{\bar{\delta}_{2M}^q} \end{bmatrix} \begin{bmatrix} \Delta C^q \\ \Delta\omega^q \end{bmatrix} = \begin{bmatrix} \bar{\delta}_1^q \\ \vdots \\ \bar{\delta}_{2M}^q \end{bmatrix}$$

which, due to good results obtained from solving the smaller problem in (26), was not pursued in this study.

4 Case Study I: A 2DOF System

This section first demonstrates how the MMC algorithm modifies a periodic solution host to match a periodic solution of a system. Then, we will examine convergence properties of the two proposed versions of the MMC algorithm and provide a comparison with a widely used Shooting algorithm in terms of radius of convergence and speed. In this regard we choose a familiar two DOF system

$$\begin{bmatrix} \ddot{x}_1 \\ \ddot{x}_2 \end{bmatrix} = \begin{bmatrix} -2 & 1 \\ 1 & -2 \end{bmatrix} \begin{bmatrix} x_1 \\ x_2 \end{bmatrix} + \begin{bmatrix} -\frac{1}{2} & 0 \\ 0 & 0 \end{bmatrix} \begin{bmatrix} x_1^3 \\ x_2^3 \end{bmatrix}, \tag{27}$$

which has been extensively studied in [24, 25, 17, 3]. This oscillator is known to have branches of periodic obits, sometimes called nonlinear modes of vibration [28, 17] that have been calculated both analytically and numerically[3].

4.1 Homogenous Convergence

Figures 3 and 4 illustrate how the proposed MMC algorithm allows one to find the Coefficients of a Fourier series expansion of a periodic solution of the system and its period by gradually modifying both the Coefficients and the period of the solution host. We refer to this type of convergence, where all the pairs of collocation points converge to

one periodic solution of the system, as a homogenous convergence. In this example, the algorithm was initiated at the point $y = [1.905, 0.9253, 0, 0]^T$ due to randomly generated coefficients of the initial Fourier series expansion, $A_{ij}^{(0)}$ with $B_{ij}^{(0)} = 0$ and $T(0) = 19.35$. The control parameters were set to $r_c^{(0)} = 1e-6$, $r_w^{(0)} = 1e-8$, $N = 10$, $M = 20$, $\delta = 0.05$ and $\sigma = 0.9$.

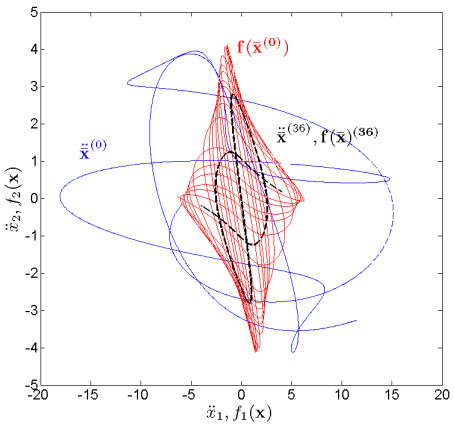

Figure 3. The acceleration and force vectors, i.e. $\ddot{x}$ and $f(x)$, of the candidate solution.

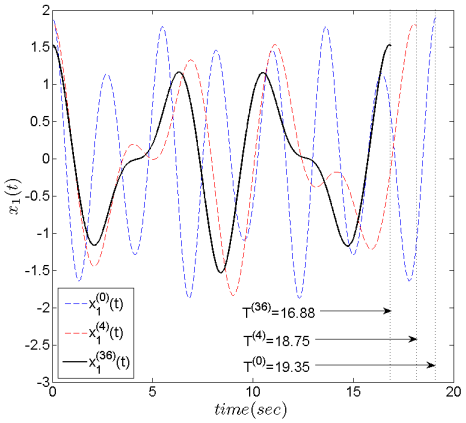

Figure 4. The displacement is shown for the candidate solution $x_1^{(k)}(t)$ where it matches the true periodic orbit of the system with $x_1^{(36)}(t)$.

As shown in Fig. 3, the initial acceleration of the solution host, i.e. $\ddot{\bar{x}}(0)$, and the force provided by the vector field, i.e. $f(\bar{x})$ generate disparate shapes initially. However after $K = 36$ steps in the direction provided by (15), those two converge to an identical shape. This convergence, elaborated in Fig. 4, is a result of considerable change in both coefficients of the Fourier series (shape and amplitude) and the period (length) of the solution host. The initial guess, which had a period of $T = 19.35$, changes as the candidate solution navigates to a periodic orbit of the system, i.e. toward satisfying (12), until it converges to a periodic solution with the period $T = 16.88$.

4.2 Radius and Speed of Convergence

The MMC algorithm seems to have a large radius of convergence especially using the conjugate gradient version. For instance, Fig. (5) shows that the the candidate solution (in the previous example) converges to a periodic orbit that is quite far from its initial start point in the state space and its initial period.

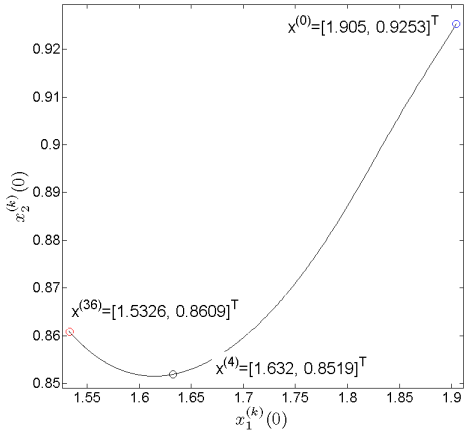

Figure 5. The path of candidate solution in the state space as it converges to a periodic orbit of the system.

To further clarify this feature, we compare the radius and speed of convergence of the conjugate gradient version of MMC (MMC-CG), it's Newtonian counterpart (MMC-N) and a shooting algorithm proposed in [21] for the same initial guess comprised of both initial conditions and periods. To do this, the coefficients $A_{ij}^{(0)}$ were selected for MMC-CG and MMC-N and then the equivalent state vector at $t = 0$ was found and used to initiate Shooting. Tables 1 and 2 show the initial conditions, period and the results for two types of typical scenarios where the initial guesses are far from any or extremely close to a periodic solution of the system (27), respectively.

Set I- In this set, the initial guess contains the initial conditions of a periodic solution with its (initial) period chosen far from the actual period ($T^{(0)} = 19.1337 \ll T^* = 40.85$). The results show that MMC-CG was able to converge to different periodic solutions (including the initial guess with the correct period) depending on what values the user chooses for the algorithm's parameters. For instance, by choosing a very small step size for the coefficients and a much larger step size for the period of the solution host, i.e. setting $r_c = 1e-12$ and $r_w = 1e-3$, the MMC-CG was able to find the a period that produced a solution close to the initial state. In contrast, as shown in Fig.5, choosing larger coefficient and smaller period step sizes, i.e., $(r_c.r_w) = \{(1.33e-8, 1e-6), (2e-8, 1e-8), (1.33e-7, 1e-8), (1e-6, 1e-8)\}$ and

$(\delta, \sigma) = (0.05, 0.9)$, led to finding periodic solutions farther form the initial guess.

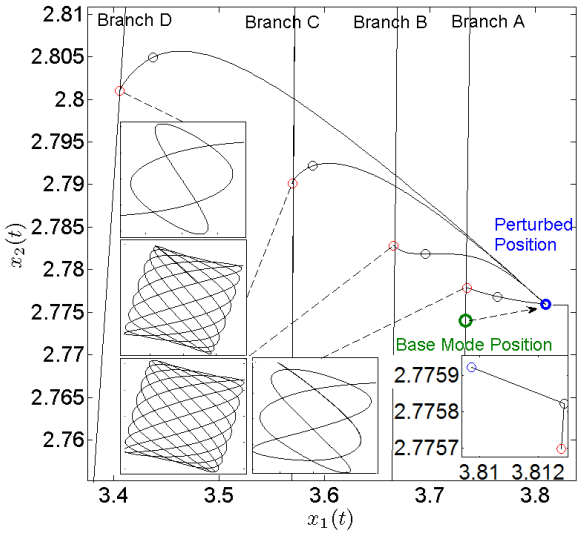

Figure 6. The path of candidate solution host in the state space as it converges to a periodic orbit of the system using the MMC-CG. (blue) initial guess, (black) intermediate result, (red) final solution. For different sets of parameters, the MMC-CG algorithm converged to different solutions on different branches of periodic solutions previously found in [3, 4].

These extreme cases show how large the radius of convergence is for MMC-CG, and while this proves the versatility of the algorithm, they come at the price of large number of steps (iterations) and slower CPUTime as outlined in Table 1. In the cases of the MMC-N or Shooting algorithms, if the algorithm converged, it always converged to the same solution regardless of its settings. However, because of the length of the solution host in the MMC algorithm, i.e. $2T$, the MMC-N (and also MMC-CG) are capable of (prone to) converging to symmetric periodic solutions, i.e. $x(t) = x(T^* - t)$, with half periods $T = T^*/2$. Case 2 in the Table 1, shows such a convergence. In this comparison set, the Shooting algorithm did not converge to any solution.

Set II- While the previous set was mainly concerned with the radius of convergence of the three algorithms, in this set, we focus on speed of convergence. All algorithms were initiated extremely close to a periodic solution of the system in (27), i.e. by applying a 0.005% relative error to the initial condition and the period of the solution. The solutions, CPU time and number of iterations are shown in Table 2. Since the MMC algorithms do not require integration, both the CG and (even more so) the Newtonian versions proved to be faster than the Shooting algorithm, although MMC-CG usually required more steps to converge to a solution. It is important to note that the CPUTime numbers given here should only be used as a rough reference. One cannot robustly evaluate speed without also comparing accuracy, which turns out to be quite challenging here because the algorithms describe the response differently, sometimes converge to very different solutions, and, in the case of MMC, may converge to multiple solutions if heterogeneous convergence is obtained. Speed and accuracy will be explored more rigorously in a future work.

Case	Method	Final State/Period	CPUTime	Iter'ns
1.1	MMC-CG	[3.4054,2.8010,0,0]/ 13.9930	3.2500	190
1.2	MMC-CG	[3.5693,2.7901,0,0]/ 45.9210	11.4375	540
1.3	MMC-CG	[3.6657,2.7828,0,0]/ 50.27310	27.7969	1592
1.4	MMC-CG	[3.7351,2.7779,0,0]/ 18.2131	24.5156	1085
1.5	MMC-CG	[3.8097,2.7759,0,0] /40.85	0.0831	8
2	MMC-N	[3.8128,2.7757,0,0]/ 20.4403	0.1250	5
3	Shooting	Did Not Converge*	-	-

Table 1. Comparison Set I- All algorithms were initiated at $y^{(0)} = [3.8097, 2.7759, 0, 0]$, $T^{(0)} = 19.1337$ as the initial (equivalent) guess of initial conditions/period. A true periodic solution exists with the initial conditions $y^{(0)} = [3.8097, 2.7759, 0, 0]$ and period $T^* = 40.85$. The MMC-CG converges to five different solutions provided different sets of step sizes.
* The algorithm was terminated after 1200 iterations.

Case	Method	Final State/Period	CPUTime	Iter'ns
1	MMC-CG	[-7.891622796236744, -32.5466172913094,0,0] /4.467174194952996	0.5313	16
2	MMC-N	[-7.891588095980071, -32.5465986978077,0,0] /4.467174782378451	0.1563	6
3	Shooting	[6.555046013403119, 47.6580858905036,0,0] /4.467174837304333	2.0625	7

Table 2. Comparison Set II- All algorithms were initiated at $y^{(0)} = [-7.891535147520359, -32.546593569114329, 0, 0]$, $T^{(0)} = 4.467174837304333$ as the initial (equivalent) guess of initial conditions.

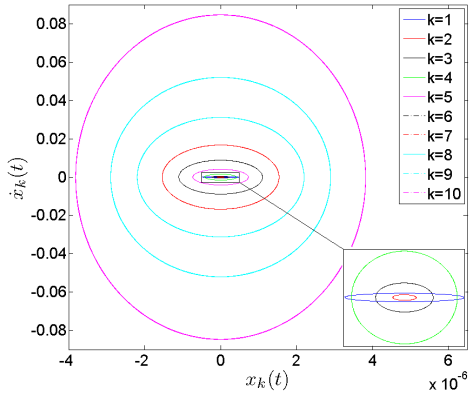

Figure 8. A periodic solution of the system (28) found after a homogeneous convergence.

5 Case Study II: A 10DOF System

To explore the scalability of the algorithm, it was also applied to a more complicated system with 10 DOF and thousands of parameters. This system also exhibits numerous cases of heterogeneous convergence and thus is an informative example. This system, shown in Fig.7, consists of a geometrically nonlinear beam, that is modeled in the Abaqus software resulting in 123 degree-of-freedom finite element model for the structure., coupled with a torsional spring at one end. Then, using an approach explained in [1], the dimension of the system was reduced. The mentioned procedure led to a ten-dimensional reduced order model that is described by

$$\begin{aligned} \ddot{x} &= f(x) \\ &= K_l x + \frac{1}{2}K_{nl1}(x_i)x + \frac{1}{3}K_{nl2}(x_i x_j)x,\ i,j = 1,...,10, \end{aligned} \tag{28}$$

where K_l is a constant matrix defining the linear part of the vector field and K_{nl1} and K_{nl2} are function matrices that define the quadratic and cubic parts of the vector field, respectively. This system was studied in more detail in [19]. For the purposes of this study, this reduced model will be considered the truth model and any approximation made in representing the structure with a 10 DOF model is irrelevant.

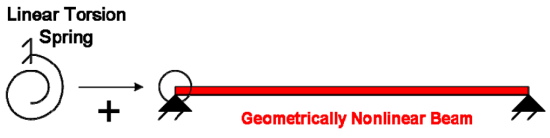

Figure 7. The ten DOF system is a reduced order model of a a geometrically nonlinear beam coupled with a linear torsional spring.

The proposed method was applied to this system and several cases of homogenous convergence were found using MMC-N with randomly generated set of initial Fourier series coefficients $A_{ij}^{(0)}$, with $B_{ij}^{(0)} = 0$. One such solution is shown in Fig. 8. The response is dominated by coordinate 5, corresponding to the 5th linear mode of the beam, yet it also shows participation of many of the other coordinates due to the strong geometric nonlinearity that is captured in the model.

5.1 Heterogeneous Convergence

This system also exhibited the interesting case where the M collocation points on the solution host land on more than one periodic orbit of the system. In such cases, although all the collocation points are guaranteed to be on periodic solutions of the system, because they satisfy (12), the candidate solution (and its period) will not match any of the final periodic solutions (or their periods). This can occur because the periodic solution host (by construction) only satisfies the equation of motion at the collocation points, but it does not guarantee that it is satisfied away from the collocation points nor does it require that the collocation points all correspond to one solution of the system. To illustrate such a situation, we present a case where the candidate solution converges to three different periodic orbits.

In this regard, Fig. (9) shows the $x_1(t)$ component of the (final) candidate solution and five resultant periodic orbits, three of which are distinct. These were found by integrating the equation of motion over one period, initiating at the state given by each of the collocation points (at time zero) and then integrating over the period defined by the solution host. This shows that, although all 5 points satisfy the condition (12), they converged to three different periodic orbits. Furthermore, as stated before, the (final) candidate solution does not (and cannot) match any of the periodic solutions.

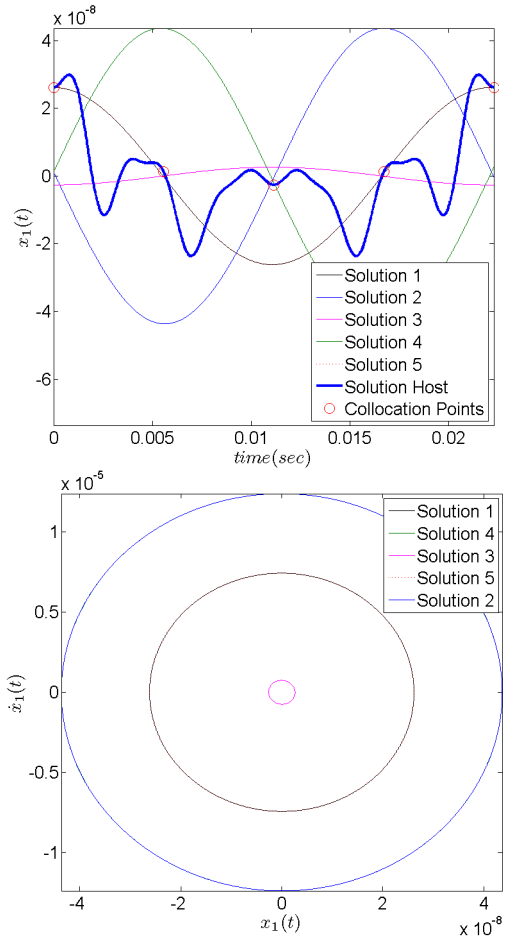

Figure 9. A case of heterogeneous convergence. The 5 pairs of collocation points converge on three different periodic solutions. Note that each of the solutions 1 through 5 were computed by integrating the equations of motion from the collocation points indicated, but starting at time zero, so the solutions do not necessarily intersect the solution host at the collocation point.

Note that if heterogeneous convergence does occur, then one does not immediately know the period of the solutions that have been obtained. This could be remedied in several ways. First, one can check for heterogeneous convergence simply by calculating $\bar{\delta}_k(\bar{x})$ at additional points between the collocation points. If $\bar{\delta}_k(\bar{x})$ is not close to the tolerance then it is likely that such a case has been obtained. If one suspects that the solution host is not a single solution on the full period T then one way to remedy the situation is to integrate the equations of motion over multiple integer fractions of the period and then to check whether the solution is periodic on any of the trial periods. This approach was used in the following to determine how many unique solutions had been obtained.

Table 3 shows that one finds even more periodic solutions as the number of pairs of collocation points increases. Furthermore, it seems that increasing the number of collocation points affects the CPUTime and the number of iterations in a sub-linear manner. Figure 10 shows the periodic solutions corresponding to the first pairs of collocation points in the second and third cases represented in Table 3 respectively.

Case	# Colloc'n Points	# Sol'ns	CPUTime	Iter'ns
1	5	3	0.0713	3
2	20	14	0.1406	3
3	50	37	0.2656	3

Table 3. Increasing number of collocation points leads to more periodic solutions on the solution host without usually affecting number of iteration required by MMC-N to converge.

It is interesting to consider what regions of the solution space are captured in each set of solutions of the MMC algorithm. One convenient way of characterizing the solution space is to use a frequency-energy plot where the frequency and total conserved energy in the solution are shown. Continuation algorithms are often used to determine how the frequency and energy of the low-energy linear modes of the system evolve with increasing energy, and all of this information can be readily shown on the frequency energy plot.

All periodic solutions of any system that (locally) satisfies the Implicit Function Theorem (IFT) will generate a continuous branch of periodic solutions [16, 8, 15, 26]. Continuation is a numerical process where a slightly changed state of a known solution is used to approximate the next solution on a continuous branch of periodic solutions[2, 9, 11, 18, 21]. The set of known solutions are very limited and usually only includes the periodic orbits of the underlying linear linear system at very low energies. In this sense, the MMC algorithm can be extremely helpful, first, by providing a rich set of initial known solutions that is not limited to the periodic orbits of the underlying linear system. Second, since it does not require integration of the equations of motion, so it may time needed to search for a solution at each point [9, 10, 17].

In this regard, Fig. 11 shows 6 branches of periodic solutions (continuations of the periodic solutions, or linear modes, of the underlying linear system, obtained using a Shooting-based continuation algorithm) and multiple discrete solutions found on each solution host using MMC-N. One can use the initial conditions of a linear periodic solution $\bar{y}_0$ to initiate MMC directly on its branch by forcing the constraint $\sum_{j=1}^{N} A_{ij} = \bar{x}_{i_{(0)}}, \sum_{j=1}^{N} B_{ij} = \frac{T^*}{2\pi}\dot{\bar{x}}_{i_{(0)}}\, i = 1,...,n$ where T^* is the period of the mentioned solution. The coefficients then were perturbed as explained for simulations performed in Set II of Section 4.2 (with 0.01 relative error). This way, the MMC-N algorithm was initiated on the aforementioned branches of periodic solutions and close to the linear solution with the highest energy with 45 pairs of collocation points. Note that, by initiating the MMC algorithm around a solution with the highest energy in the (locally) linear regions[3], one allows the collocation points to converge

[3] Any region with a very small change in fundamental frequencies of

on solutions with lower energies that share the same fundamental frequencies. This procedure was repeated 8 times resulting in 8 solution hosts, where each contained between 4 to 17 distinct periodic solutions. The solutions found on each of the mentioned solution hosts are shown with alike markers on top of their corresponding branches of periodic solutions in Fig. 11. Moreover 7 sets of solutions obtained using MMC-N with random initial settings reveal cases of internal resonances (shown in the magnified view) . These solutions are easily overlooked by shooting-based continuation algorithms; continuation tends to follow only the primary branches [3].

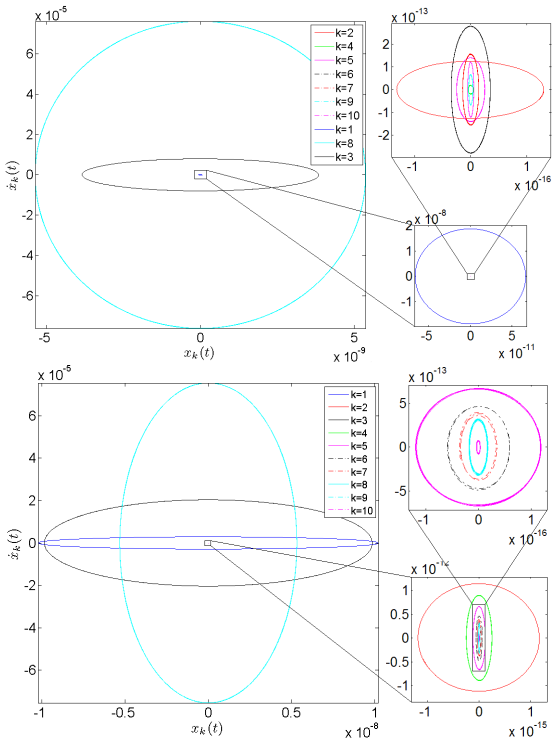

Figure 10. Phase portraits of the first periodic solutions on the solution hosts in two cases (of 14 and 37 respectively) shown in Table 3. Top: case 2. Bottom: Case 3

For instance, region A in Fig. 11 contains two periodic solutions found with MMC-N. The first solution, marked with a circle in Fig. 11 is shown in Fig. 12. This solution is identical to one found by the shooting-based continuation and represents a periodic solution associated to the first mode of vibration of the system (28). The second periodic solution, marked with a star in Fig. 11 is shown in Fig. 13 and exhibits a series of internal resonances ranging from 1:5 internal resonance (between the first and the fifth coordinate) to 1:18 internal resonance between the first and the eighth coordinates as evident in the provided time response. However, this solution cannot be found using a Shooting-based continuation algorithm unless the bifurcation point and the type of bifurcation are accurately known[3, 4]. Furthermore, since the MMC algorithm is capable of finding multiple solutions using one shared solution host it is intrinsically compatible of discovering multiple branches of periodic solutions at once.

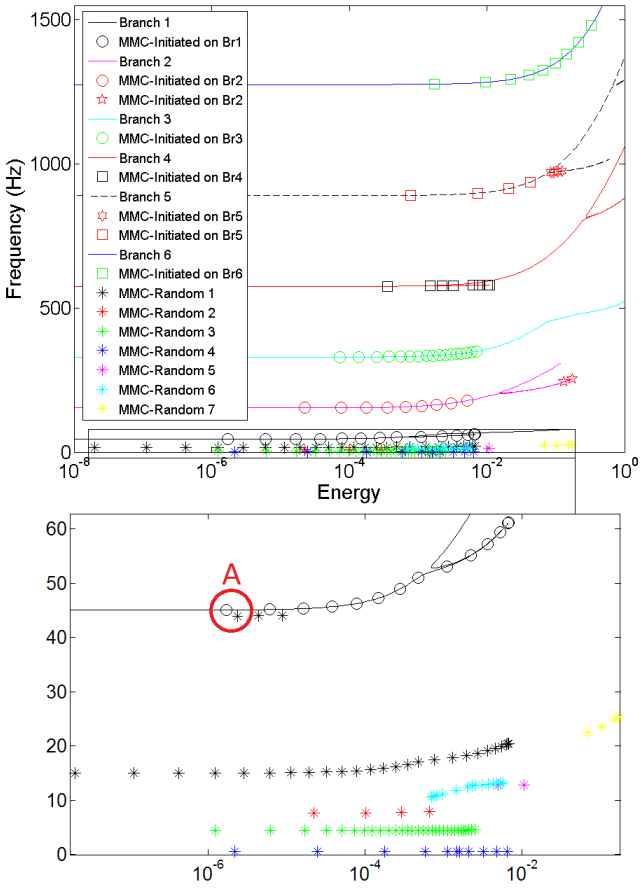

Figure 11. Frequency-energy representation of periodic solutions of the system in Eq. (28) using a Shooting-based continuation algorithm (6 branches of periodic solutions) and MMC-N. Multiple discrete solutions, found on each solution host, are shown with similar markers.

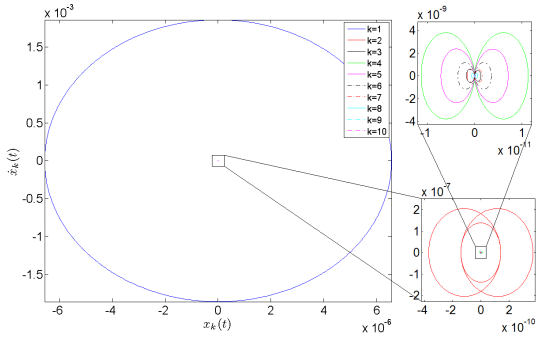

Figure 12. Phase portraits of the periodic solution ($T = 0.02225\,sec$) of the system in Eq. (28) marked with a circle on Branch 1 in region A.

periodic solutions. At lower energies, these regions are quite large and as the energy of the solutions increase, they become smaller.

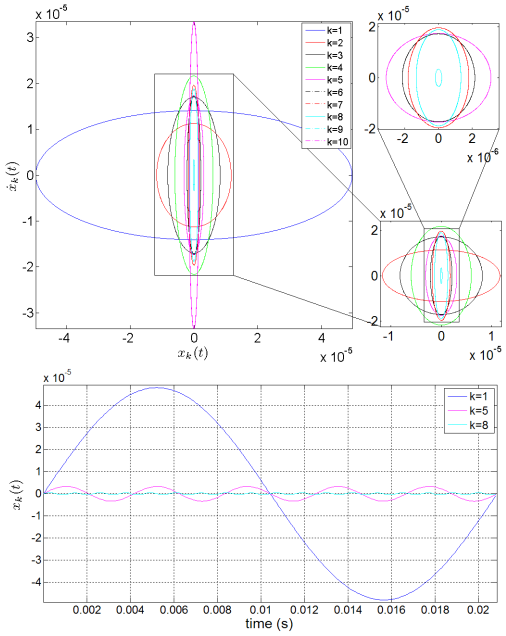

Figure 13. Top: Phase portraits of the second periodic solution ($T = 0.023\,sec$) of the system in Eq. (28) in region A. Bottom: This solution represents a case with multiple internal resonances. The time history of the response reveals cases of 1:5 and 1:18 internal resonances between the first and the fifth and also the first and the eight coordinates respectively.

6 Conclusion and Future Work

In summary, we have presented a simple yet effective method for finding periodic orbits of conservative nonlinear systems. The results obtained thus far for a small system and a relatively large system show that the method consistently converges to periodic solutions with good accuracy. The method uses a similar condition to the one used in multiple-point shooting methods, however, it does not require integration of the vector field over any period of time and is capable of finding more than one periodic orbit of the nonlinear system in each solution. Although not proven rigorously yet, the method seems to have a larger radius of convergence and to be more computationally efficient than shooting. In a future work the algorithm will be implemented in a continuation framework and further refinements will be presented.

Appendix A- Monotonicity of Multi-dimensional Multivariate Functions

In order to explain monotonicity, we begin by defining three sets for a multivariate function.

Definition I- Suppose $f : \mathbb{R}^n \to \mathbb{R}$ is C^r, $r \geq 1$, $D^n \ni u_0$ is a closed disk and $f(u_0) = p_0$. Then the level set, super-level set and sub-level set of the function f at the point u_0 are respectively defined as the sets

$$\mathcal{L}_{u_0} = \{u | f(u) = p_0, u \in D^n\},$$
$$\mathcal{L}^+_{u_0} = \{u | f(u) \geq p_0, u \in D^n\} \text{ and}$$
$$\mathcal{L}^-_{u_0} = \{u | f(u) \leq p_0, u \in D^n\}.$$

In order to simplify the notation, in the following discussion, we will refer to the above sets as $\mathcal{L}$, $\mathcal{L}^+$ and $\mathcal{L}^-$. For example, consider the multivariate function $f(x,y) = 2x^2 - y - \frac{1}{2}x^3$.

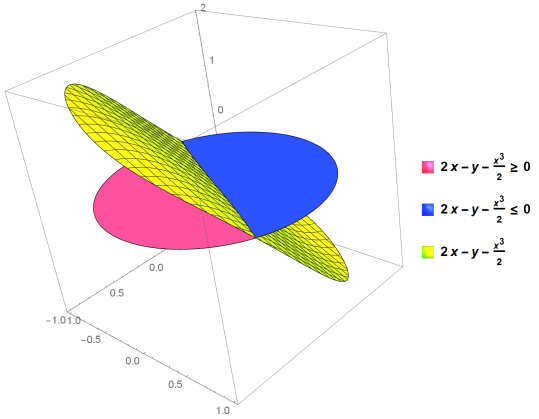

Figure 14. On the closed disk define by $D^2 = \{(x,y) \in \mathbb{R}^2 | x^2 + y^2 \leq 1\}$, the blue region of the disk highlights the sub-level set and the red region highlights the super-level set. The intersection of the two is the level set.

Now we are ready to define monotonicity for multivariate functions as the following.

Definition I - Suppose $f : \mathbb{R}^n \to \mathbb{R}$ is C^r, $r \geq 1$, D^n is a closed disk. The function f is monotone at $u_0 \in D^n$ if the sets $\mathcal{L}^+/\mathcal{L}$ [4] and $\mathcal{L}^-/\mathcal{L}$ are both simply connected.

Note that, the vector ∇f is always perpendicular to the level-set unless

The level set is a direct sum of multiple manifolds, e.g. two curves crossing at u_0 as shown in Fig. 15.
The level set is a single point, e.g. like the point $u_0 = (0,0)$ for the function $f = e^{-(x^2+y^2)}$,

which both are excluded by the above definition.

[4] Note that $A/B \equiv A - A \cap B$.

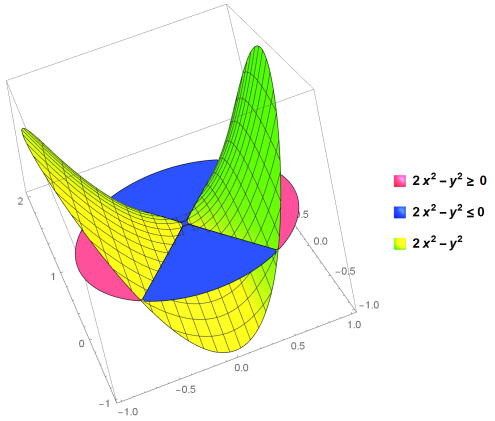

Figure 15. On the closed disk define by $D^2 = \{(x,y) \in \mathbb{R}^2 | x^2 + y^2 \leq 1\}$, the blue region of the disk highlights the sub-level set and and the red region highlights the super-level set. The intersection of the two is the level set.

As it's evident in the above figure, neither of sets $\mathcal{L}^+/\mathcal{L}$ and $\mathcal{L}^-/\mathcal{L}$ are connected. This fact can be further illustrated In Fig. 16. Next, we can define monotonicity for multi-dimensional multivariate functions as the following.

Definition II - Suppose$f : \mathbb{R}^n \to \mathbb{R}^m$ is C^r, $r \geq 1$, D^n is a closed disk. The function f is monotone at $u_0 \in D^n$ if all $f_i, i = 1,..,m$ are monotone at u_0 and $\mathcal{L}_i \pitchfork \mathcal{L}_{j\neq i}$, $i, j \in \{1,...,m\}$[5].

For example, suppose $f(x,y) = [2x - y - \frac{1}{2}x^3, 2y - x]^T$. Also, suppose that (p,q) represents an arbitrary point in $\mathbb{R}^2$ and $[2p - q - \frac{1}{2}p^3, 2q - p] = [P,Q]$. It is readily apparent that $2x - y - \frac{1}{2}x^3$ and $2y - x$ are both monotone multivariate functions. The level set of the two functions can be defined by $\mathcal{L}_1 = \{(x,y) \in \mathbb{R}^2 | 2x - y - \frac{1}{2}x^3 = P\}$ and $\mathcal{L}_2 = \{(x,y) \in \mathbb{R}^2 | 2y - x = Q\}$. In other words, $\mathcal{L}_1$ and $\mathcal{L}_2$ define two curves (M^1 manifolds) $y = 2x - \frac{1}{2}x^3 - P$ and $y = -\frac{1}{2}(x + Q)$ with the tangent vectors $[2 - \frac{3}{2}x^2, -1]^T$ and $[-1, 2]^T$ respectively. This way, one can conclude that $\mathcal{L}_1 \pitchfork \mathcal{L}_2$ except when there exists $\alpha \in \mathbb{R}$ for which

$$\begin{bmatrix} 2 - \frac{3}{2}x^2 \\ -1 \end{bmatrix} = \alpha \begin{bmatrix} -1 \\ 2 \end{bmatrix}$$

holds. One can solve the equation above and obtain $\alpha = -\frac{1}{2}$ and also $2 - \frac{3}{2}x^2 = \frac{1}{2}$ which yields $x = \pm 1$. Thus the function f is monotone almost everywhere, i.e. everywhere but at $x = \pm 1$. In this case, the results can also be obtained by solving $\det \left| \mathbb{J}^f_{(x,y)} \right| = 0$. Of course, in the general case expressed in the Definition II, one can readily prove that for $f : \mathbb{R}^n \to \mathbb{R}^m$, if $m > n$ the f cannot be monotone everywhere. By following the above analysis, one can provide another example, i.e. the function $f(x,y) = [2x - 5y - \frac{1}{2}x^3, 2y - x]^T$, which is monotone everywhere.

[5] $A \pitchfork B$ reads the set (manifolds) A intersects the set (manifold) B.

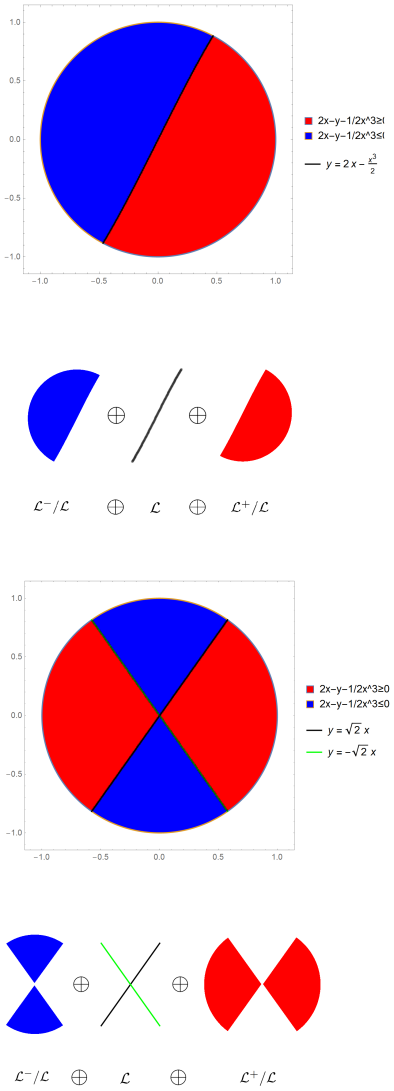

Figure 16. The disk define by $D^2 = \{(x,y) \in \mathbb{R}^2 | x^2 + y^2 \leq 1\}$ can be described by the direct sum of the sets $\mathcal{L}^+/\mathcal{L}$, $\mathcal{L}$ and $\mathcal{L}^-/\mathcal{L}$. Top: In this case the sets $\mathcal{L}^+/\mathcal{L}$ and $\mathcal{L}^-/\mathcal{L}$ are both simply connected. Bottom: In this case neither of the sets $\mathcal{L}^+/\mathcal{L}$ and $\mathcal{L}^-/\mathcal{L}$ are simply connected.

Locally Monotone and Locally Injective Functions

For a continuous single variable function, strict monotonicity implies that the function is an injection (a one to one map). As mentioned earlier, for multivariate functions, monotonicity is defined locally in the neighborhood of a point. In order to facilitate the comparison between the two properties, i.e. monotonicity and injectivity, let's define injectivity by using the concept of the level-set.

Definition- Suppose $f : \mathbb{R}^n \to \mathbb{R}$ is C^r, $r \geq 1$, D^n is a closed disk in $\mathbb{R}^n$. The function f is an injection in D^n if and only if, for every point $u \in D^n$

$$\mathcal{L}_u = u. \tag{29}$$

With this alternative form of the definition of injectivity,

it is clear that non-constant multivariate functions cannot be injective. For instance, for a function of two variables, i.e. $f(x,y)$, the above definition demands that the following equation

$$f(x,y) = c, \tag{30}$$

to always have a single solution $\{(x_0,y_0)|f(x_0,y_0) = c\}$. In other words, every point $u_0 = (x_0,y_0)$ in a closed disk D^2 must represent a local extrema, i.e $\nabla^f_{(x,y)}(u_0) = 0$.
This definition can be readily extended to multi-dimensional multivariate functions as it follows.
Definition- Suppose $f : \mathbb{R}^n \to \mathbb{R}^m$ is C^r, $r \geq 1$, D^n is a closed disk in $\mathbb{R}^n$. The function f is an injection in D^n if and only if, all f_i are injections in D^n.

One can confirm that the same discussion, presented above, about injectivity of multivariate functions also holds for multi-dimensional multivariate functions. Therefor, non-constant multi-dimensional multivariate functions cannot define injections.

Acknowledgment

The authors would like to thank Dr. R. J. Kuether for providing the reduced order model used in the second case study.

References

[1] M. S. Allen, R. J. Kuether, B. J. Deaner, and M.W. Seracic. A numerical continuation method to compute nonlinear normal modes using modal coordinates. *53rd AIAA/ASME/ASCE/AHS/ASC Structures, Structural Dynamics, and Materials Conference, Honolulu, Hawaii*, 2012.

[2] E.L. Allgower and K. Georg. *Numerical continuation methods*, volume 33. Springer-Verlag Berlin, 1990.

[3] H. A. Ardeh and M. S. Allen. instantaneous center manifolds and nonlinear modes of vibrations. In *Proceedings of the ASME 2012 International Design Engineering Technical Conferences & Computers and Information in Engineering Conference*. ASME, 2012.

[4] H. A. Ardeh and M. S. Allen. Investigating cases of jump phenomenon in a nonlinear oscillatory system. In *IMAC XXXI A Conference and Exposition on Structural Dynamics, Anaheim, CA*, 2013.

[5] Viorel Barbu. *Nonlinear differential equations of monotone types in Banach spaces*. Springer Science & Business Media, 2010.

[6] Heinz H Bauschke and Patrick L Combettes. *Convex analysis and monotone operator theory in Hilbert spaces*. Springer Science & Business Media, 2011.

[7] P. Blanchard, E. Brüning, and G.M. Hayes. *Variational methods in mathematical physics: a unified approach*. Springer-Verlag, 1992.

[8] Geoffrey Butler, HI Freedman, and Paul Waltman. Uniformly persistent systems. *Proceedings of the American Mathematical Society*, pages 425–430, 1986.

[9] AR Champneys, TF Fairgrieve, YA Kuznetsov, B. Sandstede, and XJ Wang. Auto97: Continuation and bifurcation software for ordinary differential equations, 1997.

[10] A. Dhooge, W. Govaerts, and Y.A. Kuznetsov. Matcont: a matlab package for numerical bifurcation analysis of odes. *ACM Transactions on Mathematical Software (TOMS)*, 29(2):141–164, 2003.

[11] E.J. Doedel. Lecture notes on numerical analysis of nonlinear equations. *Numerical Continuation Methods for dynamical systems*, pages 1–49, 2007.

[12] Reeves Fletcher and Colin M Reeves. Function minimization by conjugate gradients. *The computer journal*, 7(2):149–154, 1964.

[13] Roger Fletcher. *Practical methods of optimization*. John Wiley & Sons, 2013.

[14] Roger Fletcher and Michael JD Powell. A rapidly convergent descent method for minimization. *The Computer Journal*, 6(2):163–168, 1963.

[15] Jack K Hale and Paul Waltman. Persistence in infinite-dimensional systems. *SIAM Journal on Mathematical Analysis*, 20(2):388–395, 1989.

[16] H.B. Keller. Numerical solution of bifurcation and nonlinear eigenvalue problems. *Applications of bifurcation theory*, pages 359–384, 1977.

[17] G. Kerschen, M. Peeters, J.C. Golinval, and AF Vakakis. Nonlinear normal modes, Part I: A useful framework for the structural dynamicist. *Mechanical Systems and Signal Processing*, 23(1):170–194, 2009.

[18] B. Krauskopf, H.M. Osinga, and J. Galán-Vioque. *Numerical Continuation Methods for Dynamical Systems: Path following and boundary value problems*. Springer, 2007.

[19] Kuether. Structural modification of nonlinear fea subcomponents using nonlinear normal modes. In *International Modal Analysis Conference (IMAC XXXI) Garden Grove, CA*, 2013.

[20] A.H. Nayfeh. *Introduction to perturbation techniques*. Wiley-VCH, 2011.

[21] M. Peeters, R. Viguié, G. Sérandour, G. Kerschen, and J.C. Golinval. Nonlinear normal modes, part ii: Toward a practical computation using numerical continuation techniques. *Mechanical systems and signal processing*, 23(1):195–216, 2009.

[22] MJD Powell. Nonconvex minimization calculations and the conjugate gradient method. In *Numerical analysis*, pages 122–141. Springer, 1984.

[23] S.M. Roberts and J.S. Shipman. *Two-point boundary value problems: shooting methods*. American Elsevier Publishing Company, 1972.

[24] R.M. Rosenberg and C.P. Atkinson. On the natural modes and their stability in nonlinear two-degree-of-freedom systems. *Journal of Applied Mechanics*, 26:377–385, 1959.

[25] S.W. Shaw and C. Pierre. Non-linear normal modes and

invariant manifolds. *Journal of Sound and Vibration*, 150(1):170–173, 1991.

[26] J. Shi. Persistence and bifurcation of degenerate solutions. *Journal of Functional Analysis*, 169(2):494–531, 1999.

[27] Stephen Simons. *Minimax and monotonicity*. Springer, 1998.

[28] A. F. Vakakis. *Analysis and identification of linear and nonlinear normal modes in vibrating systems*. PhD thesis, California Institute of Technology, 1990.